DAMAGE ACCUMULATION DURING DUCTILE RUPTURE AND THE DEVELOPMENT OF FAILURE MAPS

D. Teirlinck*, M. F. Ashby and J. D. Embury***

**Department of Metallurgy & Materials Science, McMaster University, Hamilton, Ontario, Canada L8S 4L7*

***Engineering Department, University of Cambridge, Trumpington Street, Cambridge, England*

ABSTRACT

A variety of fracture modes can be modelled as processes of cumulative damage. A quantitative comparison of the model and the experimental data is given for ductile fracture under a wide variety of superimposed pressure. Failure maps have been constructed which permit the competition between fracture modes for various stress states to be described in a simple diagram.

KEYWORDS

Damage accumulation, void growth, shear failure, brittle failure, microcrack linkage, failure maps.

INTRODUCTION

Fracture is the end point of the plastic strain history. In the case of ductile fracture, for example, a sequence of events consisting of void nucleation, hole growth and coalescence occur, which can be regarded as a process of damage accumulation (occurring concomitantly with the process of strain hardening) leading to final failure. The evolution of the damage depends on local microstructural features such as the strength of interphase interfaces, grain boundaries etc., the operative state of stress and the stability and distribution of plastic strain in the material. Other fracture mechanisms such as cleavage, shear fracture, etc. follow similar progressions.

Thus in attempting to evaluate fracture criteria it is important to consider the competition between fracture modes in relation to the current level of flow stress in the material (and hence its detailed microstructure), and both the operative state of stress and the strain history of the material. In order to describe and quantify the competition between fracture modes as a function of stress state and specifically the level of the hydrostatic stress component, σ_M, it is useful to divide the problem into two steps. The first involves developing a cumulative damage model capable of describing the individual stages of void nucleation, growth and coalescence, together with quantitative criteria for the alternative failure modes. The second step is in essence a descriptive one but is important in achieving a

pictorial representation of the occurrence of the various fracture modes in relation to the processes of initial plastic flow and strain hardening. This involves the development of failure maps using a variety of co-ordinate systems (Teirlinck, 1983). The experimental work described in this system deals with axisymmetric deformation modes. However, failure maps can be developed for a variety of other stress states and in the final portion of this paper examples are given of the application of failure maps to other loading paths. In the failure maps the various possible fracture processes are represented by separate loci. However as stated earlier, we can consider that at large strains the material strain hardens concomitantly with the development of microstructural damage; then contours can be drawn within the failure surface, indicating level of damage accumulated at a given stress state. In this way a damage contour map can be drawn to indicate the relative rates of damage accumulated along various loading paths.

DUCTILE FRACTURE

The processes of void nucleation, growth and coalescence have been considered in a quantitative manner by several authors (Thomason, 1968; McClintock,1968; Brown and Embury, 1973). A variety of models can be used to predict properties such as the tensile strain to failure as a function of the volume fraction of second phase particles. There are, however, some detailed physical processes which are inaccessible in models of this type because of the simplifying assumptions such as the existence of a unique nucleation strain at which void growth starts, or the importance of a geometrical condition (Brown and Embury, 1973) for void linkage which constitutes failure.

In the present study, axisymmetric tensile tests have been performed at a variety of superimposed hydrostatic pressures for a 1045 spheroidized steel and the damage process monitored by quantitative metallography in order to count the number of void sites and measure the total area fraction of voids as functions of strain (Brownrigg and co-workers). In accord with previous work (Palmer and Smith, 1966; Fisher and Gurland, 1981) it has been found that void nucleation depends on the size of the carbide particles, the larger particles cavitating first. Therefore nucleation does not occur at a unique strain, but can be considered as a front which travels through the particle size distribution at a rate dependent on imposed strain and hydrostatic stress, as shown schematically in Fig. 1.

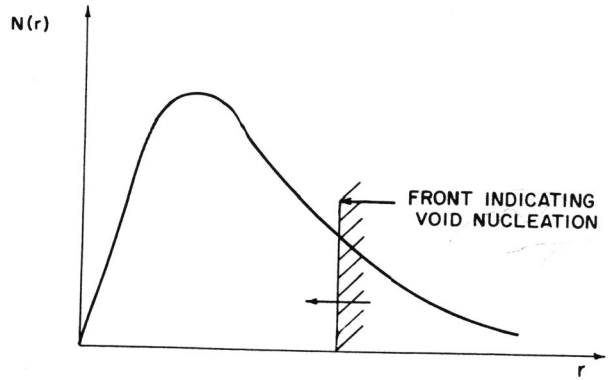

Fig. 1. Schematic diagram showing the movement of a void nucleation front through the particle size distribution.

The damage accumulation data have been analyzed by using this concept. The nucleation criterion used has been taken from Goods and Brown (1979). They have shown that the nucleation strain ε_N can be expressed as a function of the hydrostatic stress component σ_M and the interfacial strength σ_I as:

$$\sqrt{\varepsilon_N} = H(\sigma_I - \sigma_M) \tag{1}$$

where H is a constant depending on the size and volume fraction of the second phase particles. This equation can be used to determine σ_I for a given system, ε_N, being taken as the strain at which the curves giving the number of voids N as a function of strain for different stress states extrapolates to zero.

However, the constant H in equation (1) must be developed. In order to account for the experimental observations, the following empirical relationship between the dislocation density around a particle, ρ_ℓ, and its size r, has been taken (Teirlinck, 1983):

$$\rho_\ell = A \frac{\varepsilon}{b} r^q \tag{2}$$

where A is a constant, b the Burgess vector and q an exponent which has to be determined from experimental results. The critical radius for nucleation r_c is given by

$$r_c = \left[\frac{(\sigma_I - \sigma_M)^2}{H' b \varepsilon} \right]^{1/q} \tag{3}$$

where H' is a constant. If the distribution of particle sizes can be represented by a function f(r), the number of voids nucleated in an increment $d\varepsilon$ of strain is:

$$dN = N_A f(r_c) dr_c \tag{4}$$

where N_A is the number of particles per unit area. It is therefore possible to calculate incrementally the curves for different stress states and to compare them with experimental observations. This comparison is shown in Fig. 2 for the 1045 steel tested under four different levels of hydrostatic pressure. The exponent q has been determined from the curve $N(\varepsilon)$ obtained at atmospheric pressure (0.1 MPa) and subsequently used to calculate the curves $N(\varepsilon)$ at higher pressures. Its value was found to be 8. It can be seen in Fig. 2 that the model is in good agreement with the experimental results.

Once nucleated, the voids grow and the rates of increase in the direction of the tensile axis (subscript 3) and in the transverse direction (subscript 1) are given (Rice and Tracey, 1969) by:

$$dR_1 = \left(-\frac{Y}{2} + D\right) d\varepsilon \tag{5}$$

$$dR_3 = (Y + D) d\varepsilon$$

Y is an amplification factor, given by (LeRoy and co-workers, 1981):

$$Y = 1 + \exp(-2.25(\varepsilon - \varepsilon_N)) \tag{6}$$

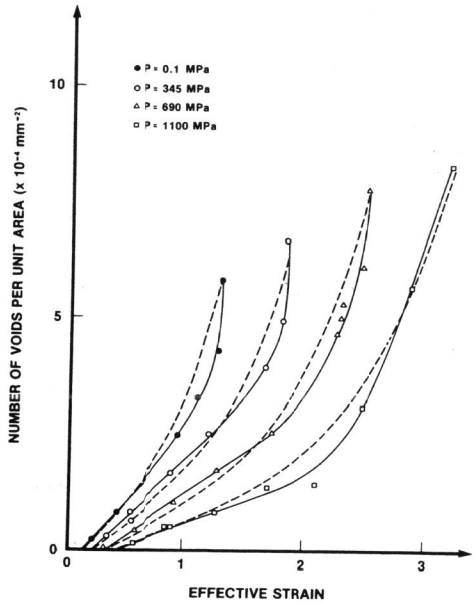

Fig. 2. Comparison of the calculated number of voids per unit area vs effective strain curves with the experimental ones for a spheroidized 1045 steel.

The factor D describes the volume change of the voids, and is given by:

$$D = 0.56 \sinh \left(\frac{3}{2}\frac{\sigma_M}{\sigma}\right) \qquad (7)$$

where σ is the flow stress of the matrix.

Introducing these equations into the previous calculations of the curves $N(\varepsilon)$ allows the determination of the damage in terms of the area fraction of voids. The calculated curves (broken lines) so obtained are compared with the experimental results (solid lines and data points) in Fig. 3. Despite some discrepancy in the steep part of the curves, the agreement is satisfactory, and in particular, the model accounts for the experimental observation that failure occurs when a critical amount of damage is reached (here an area fraction of about 4%), regardless of the superimposed pressure.

This latter observation can be taken as a fracture criterion. However, the physical meaning of this critical level of damage is unclear. It may indicate the level of damage at which either a macrocrack is formed in a geometrical manner or the dilatational work attains a critical value. Alternatively, the coalescence event could be considered as a percolation process triggered by the attainment of the critical level of damage.

Let us now consider the above models from the viewpoint of how the fracture behaviour may be modified. Clearly on a microstructural basis the simplest variable to consider is the volume fraction of second phase particles. The

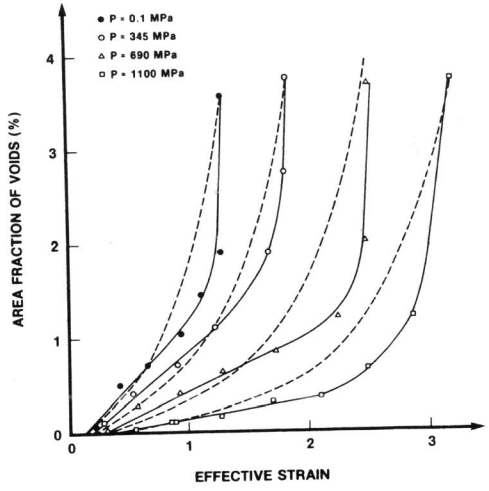

Fig. 3. Comparison of the calculated area fraction of voids vs effective strain curves with the experimental ones for a spheroidized 1045 steel.

effect of increasing the volume fraction of Fe_3C from 3% to 15% on the damage accumulation is shown in Fig. 4. However, the description of the nucleation, growth and coalescence processes given in the previous section suggest a variety of more subtle ways of influencing the fracture behaviour.

Let us consider first the nucleation process. Fracture behaviour can clearly be influenced by reducing the strain needed to initiate damage. Thus if the strength of the inclusion-matrix interface is reduced, the strain to the onset of damage is reduced as shown schematically in Fig. 5. This will be particularly important in systems containing large volume fractions of second phase particles and an example of this behaviour for dual phase steels (Kot and Morris, 1979) is shown in Fig. 6. The micrograph clearly shows that void nucleation occurs readily at the martensite-ferrite interface. In addition to varying the interfacial strength either by virtue of the nature of the second phase particle or by effects of local segregation, the nucleation process can also be influenced by the distribution of particle sizes. If we alter the form of the particle size distribution, the rate of increase of <u>both</u> the number of voids <u>and</u> the amount of damage with strain can be varied. As a simple illustration of this effect, let us suppose that we replace the log-normal distribution of particle sizes observed in the spheroidized 1045 steel with that predicted by the Wagner-Lifshitz (Rastogi and Ardell, 1971) model of coarsening.

The forms of the two distributions are shown in Fig. 7a and 7b, and they are given by

$$f(r) = \frac{\alpha}{r} \exp\left[-\frac{(\log r + \beta)^2}{\gamma}\right] \qquad (8)$$

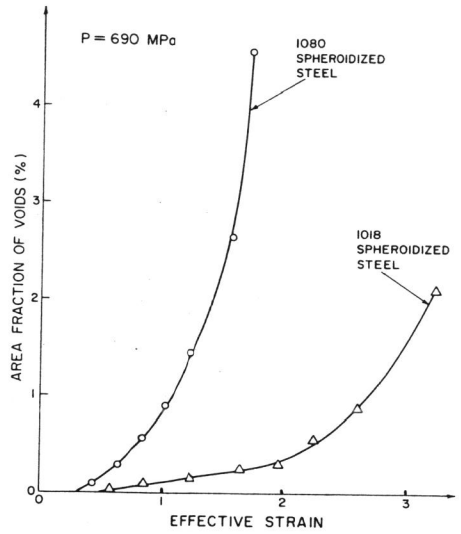

Fig. 4. Diagram showing the influence of the volume fraction of second phase particles on the damage accumulation at a superimposed pressure of 690 MPa.

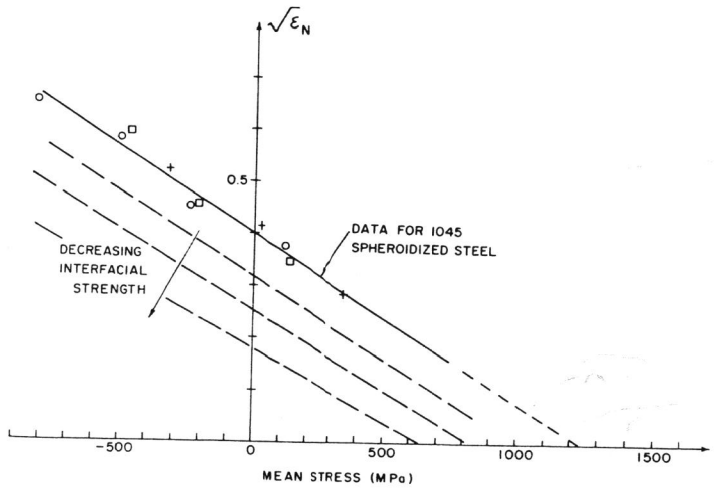

Fig. 5. Diagram showing the variation of the square root of the average nucleation strain with the hydrostatic stress component. The dotted lines represent hypothetical conditions for weaker interfaces.

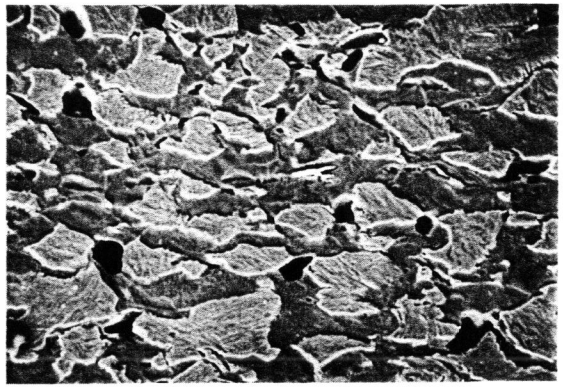

Fig. 6. SEM micrograph showing the nucleation of voids at the martensite-ferrite interface in a dual-phase steel tested in tension under a superimposed pressure of 345 MPa. ε = .44

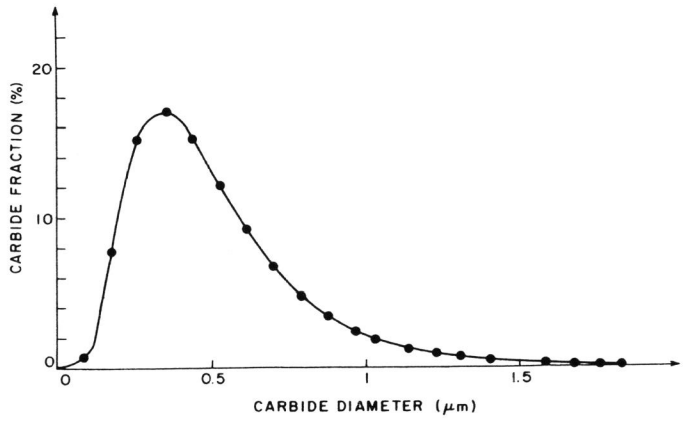

Fig. 7a. Size distributions of second phase particles: log-normal law found experimentally in a spheroidized 1045 steel.

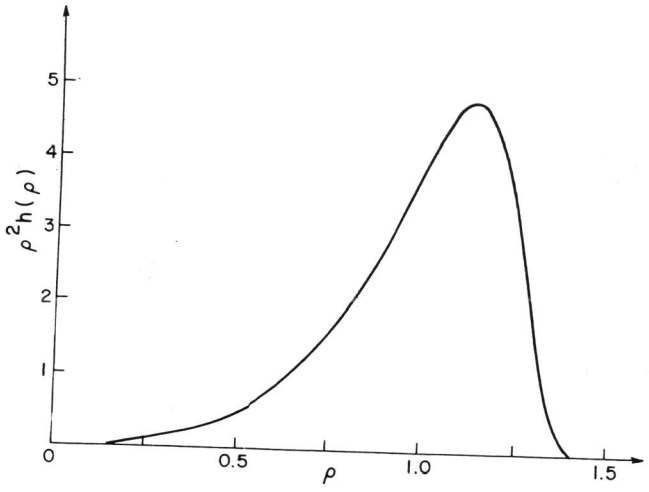

Fig. 7b. Size distributions of second phase particles: distribution obtained from the Wagner-Lifshitz coalescence model.

for the log-normal distribution, and

$$f(\rho) = \rho^2 h(\rho) \quad \text{for the Wagner-Lifshitz distribution}$$

with

$$h(\rho) = \left(\frac{3}{3+\rho}\right)^{7/3} \left(\frac{1.5}{1.5-\rho}\right)^{11/3} \exp\left(\frac{-\rho}{1.5-\rho}\right) \text{ if } \rho < 1.5 \qquad (9)$$

where $\rho = r/\bar{r}$, ($\bar{r}$ being the average particle radius) for the Wagner-Lifshitz distribution. The predicted variations of the area fraction of voids vs strain obtained with these two distribution functions are shown in Fig. 8.

It can be seen that the change in distribution function clearly accelerates the damage accumulation and reduces the fracture strain. In physical terms this arises because more of the particles are in the high region of the distribution and clearly the effect would be even more drastic with bimodal distributions. It should be emphasized that although the influence of size distribution is important, it is not necessarily the best method of describing the problem. It is well established that local aggregation of particles can sharply reduce the strain to failure (e.g. in through thickness tensile properties (Miyoshi and co-workers, 1974)). The process of particle

aggregation is an important one but the description needed is one which considers the distribution of local volume fractions rather than particle size. It is helpful to think of two components to the damage: individual voids D_s and void clusters D_{agg} (Fig. 9); the total damage is the sum of the two.

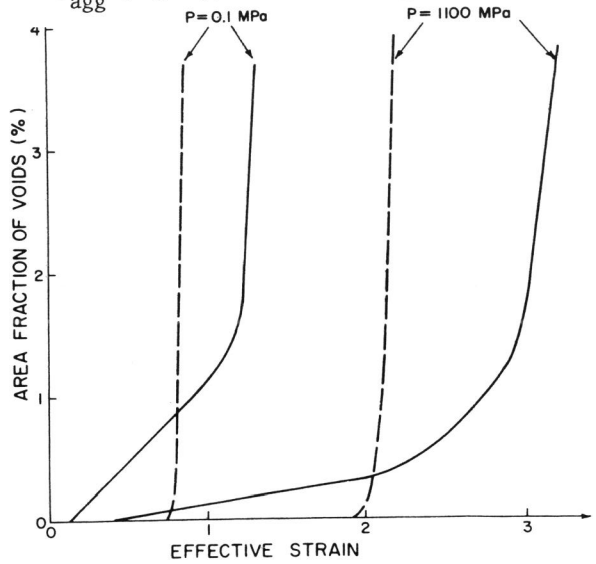

Fig. 8. Diagram illustrating the influence of the shape of the particle size distribution on the damage accumulation in a spheroidized 1045 steel. The solid curves refer to the log-normal distribution and the dotted ones to the Wagner-Lifshitz distribution.

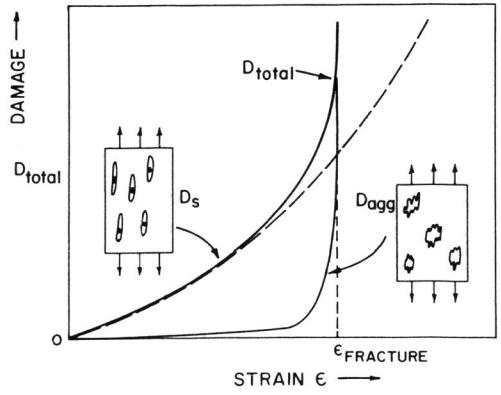

Fig. 9. Diagram showing the accumulation of damage as single voids D_s and void clusters D_{agg} as a function of strain.

For most of the life, single-void damage is dominant, but toward the end of life, local clusters of linked voids increase in number. It is these void-clusters which ultimately propagate and link to give the final fracture, truncating the process of single-void growth, as shown in Fig. 9. It is probably for this reason that the experimental damage accumulation curves shown in Figs. 2 and 3 rise more steeply towards the end of life than the simple theory predicts. The damage aggregation process may be linked to the initial clustering of particles. The incorporation of a model based on the distribution of local volume fractions would in essence outline a system of damage mechanics which would define both the level of damage needed to produce failure and the volume or size of the region over which this damage level must be sustained.

Let us now consider the variation in fracture behaviour which can be produced via the void growth process. The results in the previous section show that the growth up to the critical damage level can be retarded by the application of hydrostatic pressure. However the volume over which the damage is produced remains limited due to localized necking. For other two-phase systems (Wilkinson and Caceres) deformed at higher temperatures and lower strain rate, the matrix became superplastic enabling the damage accumulation process to change in two ways. First the critical level of damage prior to failure may be increased up to 20% (Taplin and co-workers, 1979) and secondly due to the slow rate of neck development, the damage may be dispersed over a larger volume of the sample. To appreciate the significance of the changes in damage accumulation which can occur, it is useful to emphasize that the description of damage accumulation should really be coupled with a description of the variation of material properties in the ligaments between the voids. Thus if the work hardening rate of the ligaments is increased, the material is able to either sustain greater levels of damage or to distribute the damage over a different volume of the sample. This type of approach was used by Iricibar (Iricibar, LeRoy and Embury,1980) to increase the ductility of spheroidized steels by use of a recovery anneal to restore the work hardening capacity of the material after some initial damage accumulation. In principle the changes in material properties could be accomplished by a variety of methods such as transformation hardening in metals or by gradual molecular alignment in polymeric systems.

The flow stress can be written as

$$\sigma = \sigma(\varepsilon)(1-D) \tag{10}$$

where D is a damage parameter varying from 0 to 1. Therefore

$$\frac{d\sigma}{d\varepsilon} = \frac{\partial\sigma}{\partial\varepsilon}(1-D) - \sigma(\varepsilon)\frac{\partial D}{\partial\varepsilon} \tag{11}$$

Fracture takes place when $d\sigma/d\varepsilon = 0$, thus the criterion is

$$\frac{\partial\sigma}{\partial\varepsilon}(1-D) = \sigma(\varepsilon)\frac{\partial D}{\partial\varepsilon} \tag{12}$$

It is possible to relate this simple model to the criterion for ductile fracture found for the 1045 steel tested under superimposed pressure. As the applied pressure increases, the fracture strain increases so that the strain hardening of the matrix $\partial\sigma/\partial\varepsilon$ decreases, the flow stress $\sigma(\varepsilon)$ increases slightly, and the rate of damage development decreases. Therefore,

if D is taken as the critical amount of damage for ductile fracture, the constancy of D with respect to superimposed pressure could be consistent with the condition (LeRoy and co-workers, 1981). It is, however, not possible to test this criterion as the quantities involved (strain hardening, flow stress) refer to the local values in the matrix, whereas the experiment provides only global values.

ALTERNATIVE FRACTURE MODES

Thus far consideration has been given to the influence of hydrostatic pressure on damage accumulated in ductile rupture. However, two other aspects of the pressure dependence of the failure process must be considered. These are illustrated by the sequence of micrographs shown in Figs. 10 and 11.

In Fig. 10, it can be seen that as the superimposed hydrostatic pressure increases, the central fibrous part of the fracture surface of a 1080 spheroidized steel decreases relative to the shear portion indicating that at sufficiently high pressure, the shear failure mode will take place. This has been reported by a number of other authors (Bridgman, 1952; Davidson and Ansell, 1968) and it indicates that the locus of localized shear mode must be represented on the failure map in order to establish in which stress regimes this mode is competitive with the ductile failure mode.

The second series of micrographs shown in Fig. 11 indicate the pressure dependence of a brittle fracture mode. In this case, the Fe-P alloy fails at ambient pressure and temperature by a combination of intergranular fracture and transgranular cleavage prior to necking. However, with increasing pressure the failure mode is changed and the material exhibits the production of many isolated microcracks. Thus we can surmise that the process of brittle fracture involves both the production and linkage of microcracks and hence the microcracking is in effect a cumulative damage process in which the linkage step is pressure dependent. In addition to the presence of arrested microcracks, the microcracking pattern is also altered by the large deformations obtained under hydrostatic pressure, and by the creation of a neck prior to failure. Indeed, if a crack is created at an angle less than 90^{o} to the tensile axis and then stabilized, the subsequent tensile deformation can rotate and align it along the direction of the tensile axis. In the neck, the hydrostatic tension can counterbalance the superimposed pressure, creating then a tensile stress at the tip of the vertical crack, which can open and propagate according to a mode I opening along the direction of the tensile axis. This explains the very long vertical cracks observed in the samples tested under 1100 MPa.

These observations indicate that the brittle fracture process is also pressure dependent, and can be represented by a separate locus on the failure maps.

FAILURE MAPS OF COMPETITIVE PROCESSES

In order to describe analytically different fracture criteria, failure maps have been developed which refer to an axisymmetric stress state. The stress coordinates chosen are the effective stress σ given by

$$\sigma = \left\{ \frac{1}{2}\left((\sigma_1-\sigma_2)^2 + (\sigma_2-\sigma_3)^2 + (\sigma_3-\sigma_1)^2\right)\right\}^{\frac{1}{2}} \tag{13}$$

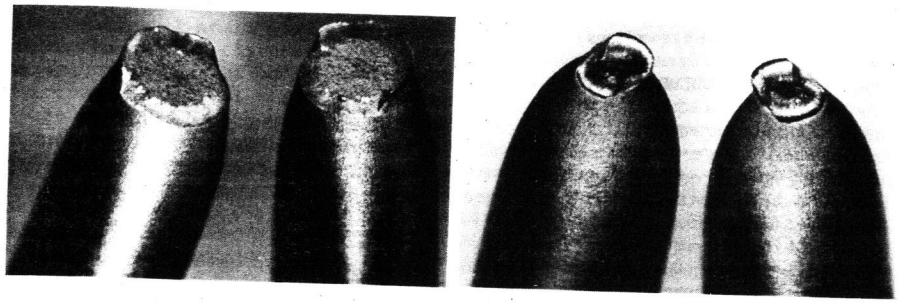

P = 0.1 MPa

P = 1100 MPa

Fig. 10. Macrophotographs of fractured samples of 1080 steel tested under various pressures.

and the superimposed pressure p. The determination of the various fracture loci, together with the plastic yielding and the onset of necking are now presented.

1. Plastic Yielding, Necking, Plastic Failure

The flow behaviour of materials is slightly pressure dependent, and it can be written as (Richmond and Spitzig, 1980),

$$\sigma = A\varepsilon^n(1 + \frac{10p}{K}) \tag{14}$$

where K is the bulk modulus, and n the strain hardening rate.

Plastic flow starts when σ exceeds the yield stress σ_y. Therefore, if σ_y^o is the yield stress at p = 0, the relationship between σ and p for plastic yielding is,

$$\sigma = \sigma_y^o(1 + \frac{10p}{K}) \tag{15}$$

Similarly, if σ_n^o is the stress at which necking starts at p = 0, the effective stress for necking is given by,

$$\sigma = \sigma_n^o(1 + \frac{10p}{K}) \tag{16}$$

with $\sigma_n^o = A\, n^n$.

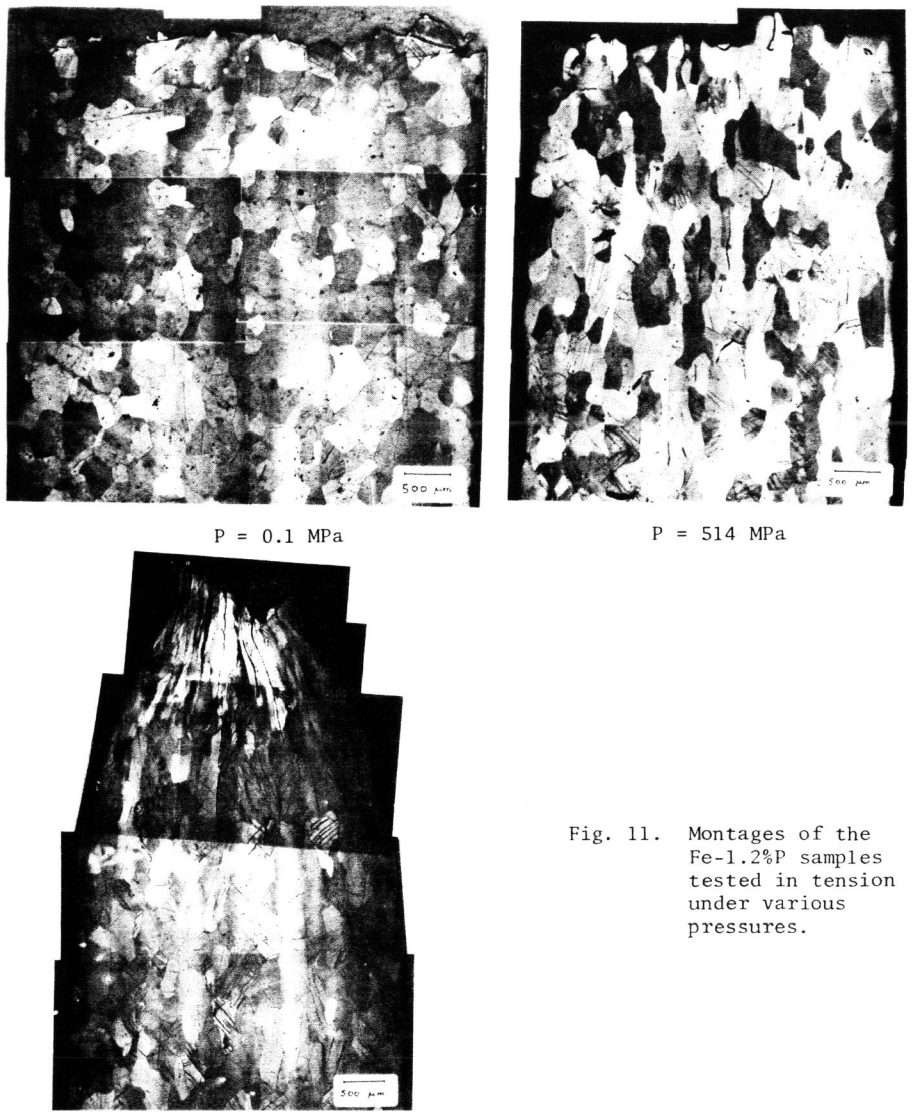

P = 0.1 MPa

P = 514 MPa

P = 1100 MPa

Fig. 11. Montages of the Fe-1.2%P samples tested in tension under various pressures.

If no other mechanism intervenes, necking leads to plastic failure: once the neck is created, flow localizes within the neck, and after a further strain of order 1, the cross-section is reduced to zero. The effective stress for plastic failure is thus,

$$\sigma = A(1+n)^n(1 + \frac{10p}{K}) \tag{17}$$

2. Ductile Fracture

The effective stress for ductile fracture can be determined approximately using the growth model of Rice and Tracey (1969) and LeRoy and co-workers (1981) together with a geometrical criterion for void coalescence (Brown and Embury, 1973).

In its simplest form the result is,

$$\sigma = \sigma^o \left[\frac{C}{1+0.56\ \sinh(\frac{1}{2} - \frac{3}{2}\frac{p}{\sigma^0})}\right]^n(1 = \frac{10p}{K}) \tag{18}$$

where C is a constant (about 2.5) and σ^0 is the ductile fracture stress at p = 0.

3. Shear Fracture, or Void Sheeting

The occurrence of a band of localized deformation between adjacent voids leading to a void sheeting failure mechanism can be analyzed using the instability criterion of McClintock(1968) and a simplified void nucleation model. The relationship between σ and p at fracture has the general form,

$$\sigma(\sigma^{1/n} - C(1 + \frac{p}{\sigma_I})^2) = \sigma^0(\sigma^{0\,1/n} - C) \tag{19}$$

where σ^0 is the fracture stress by shear failure when p = 0, C is a constant, and σ_I is the strength of the particle-matrix interface.

4. Cleavage and Brittle Intergranular Fracture

Murrel (1983) has given a relationship between σ and $\sigma_M = 1/3\ (\sigma_1 + \sigma_2 + \sigma_3)$ for brittle fracture as,

$$\sigma = 24\ \sigma_M\ \sigma^0 \tag{20}$$

truncated by the line $\sigma = \sigma^0 + \sigma_M$, where σ^0 is the fracture stress by cleavage in simple tension with no confining pressure. σ_M can be approximated to the superimposed pressure p, so that the effective stress for brittle fracture is,

$$\sigma = \sigma^0 + p \tag{21}$$

5. Construction of the Maps

The equations given above define the locus of points in σ- p space at which a given fracture mechanism results in final failure. These loci are plotted by stepping through values of p, evaluating σ at each step. The fracture mode operating at a given pressure p is the one corresponding to the lower value of σ: therefore the material fails when the inner envelope of the fracture lines is reached. Fig.12a shows the map obtained for the 1045 spheroidized steel; the inner envelope is shaded and the fracture modes are given on the top of the map.

The development of failure maps of the type described in the previous section permit consideration of the influences of factors such as local microstructural features, temperature stress state or strain path on the failure mode. Let us consider the potential use of the failure maps by a variety of examples.

6. Temperature Dependent Behaviour

In b.c.c. materials, a reduction in temperature produces a rapid increase in yield stress. However, in the ductile fracture process the loci describing void nucleation and final fracture are in essence linked to the yield surface. Thus, in b.c.c. materials, as the test temperature is reduced all the loci involving ductile rupture are expanded outwards in stress space together with the yield surface. The stress for cleavage fracture is only weakly temperature dependent (Knott, 1973) and thus as the yield surface and damage accumulation loci are expanded a variety of stress states appear in which brittle fracture can occur,as illustrated in Fig. 12b.

7. Microstructural Control

In aluminum alloys intergranular fracture can be promoted by heat treating the material so as to both raise the level of the flow stress and promote extensive grain boundary precipitation. In a high purity Al - 3.6% Cu alloy this can be accomplished by aging the material for 4 days at 125°C following quenching from solid solution. When this material is tested in tension at atmospheric pressure the fracture is intergranular,as shown in Fig. 13.

Tests under superimposed hydrostatic pressure modify the damage accumulation process and eventually enable shear fracture and plastic rupture to occur as shown in the sequence in Fig. 14. This transition in fracture behaviour can be represented by a failure map, as shown in Fig. 15.

8. Strain Path Dependence

So far in the use of failure maps we have considered the situation where the yield surface and the processes (and thus the loci) associated with plastic yielding are expanded outwards and intersect the loci for various alternative fracture modes. However, all strengthening processes cannot be considered in terms of an isotropic expansion of the yield surface. In the models of precipitation hardening due to Fisher, Hart and Pry (1953) and Brown and Stobbs (1971), rigid second phase particles can act to polarize the work hardening by producing elastic back stresses in the matrix which oppose the local unrelaxed stresses carried by the particles. In the peak aged Al-Cu system this type of hardening contributes a significant fraction

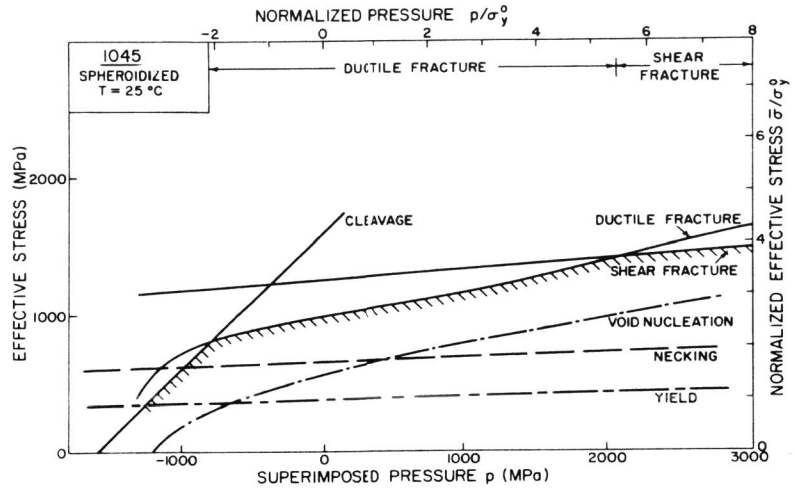

Fig. 12a. Fracture map in σ-p space for a spheroidized 1045 steel tested at ambient temperature.

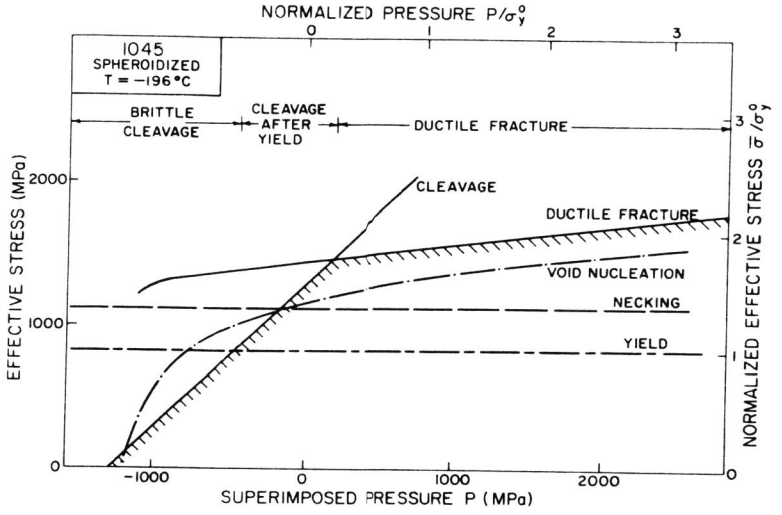

Fig. 12b. Fracture map in σ-p space for a spheroidized 1045 steel tested at -196°C.

Fig. 13. SEM micrograph of a peak aged Al-3.6% Cu tensile sample broken at atmospheric pressure.

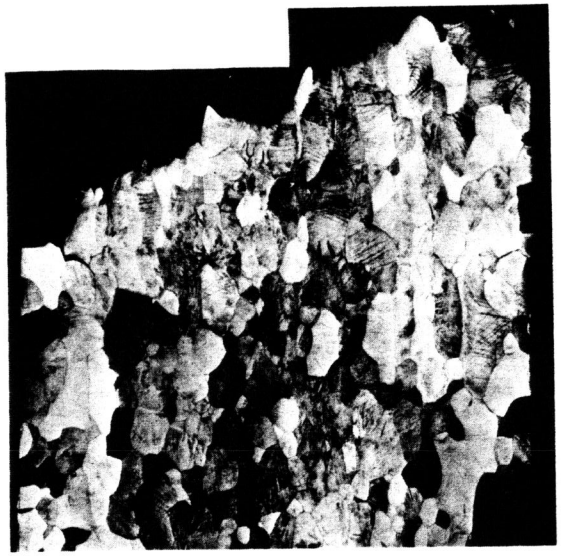

Fig. 14a. Montage of the peak aged Al-3.6% Cu tensile samples broken under various pressures: a) 0.1 MPa

Fig. 14b

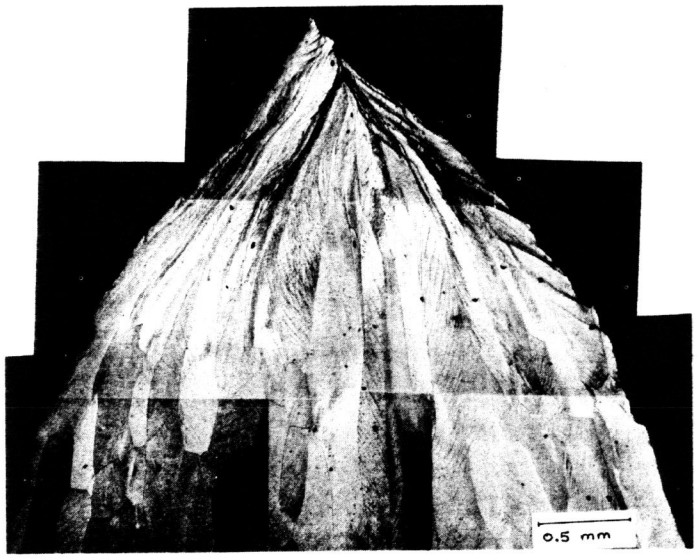

Fig. 14-c

Fig. 14b & c. Montages of the peak aged Al-3.6% Cu tensile samples broken under various pressures: b) 414 MPa, c) 690 MPa.

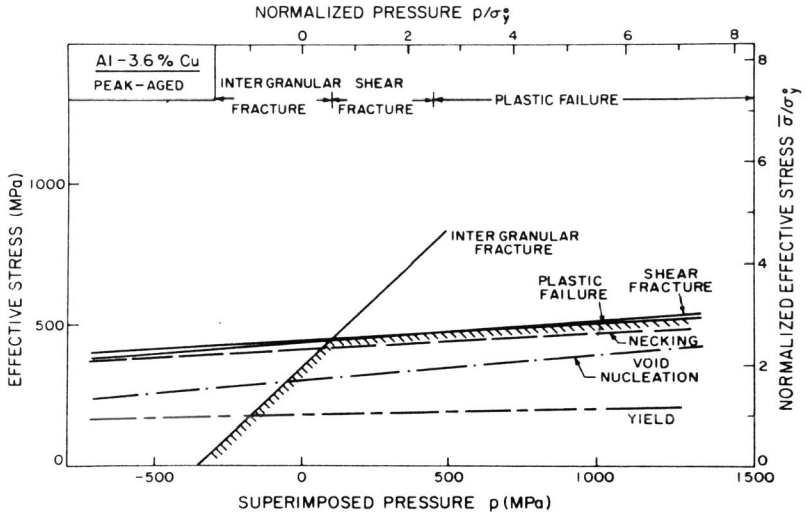

Fig. 15. Fracture map in σ - p space for the peak aged Al-3.6% Cu.

of the total work hardening (Moan and Embury, 1979). Thus it is useful to consider not only the expansion of the yield surface but its translation in stress space. For simplicity we can consider that the translation occurs in the direction of the strain vector; with this assumption we can consider the influence of simple changes in strain path such as initial deformation in compression or tension followed by deformation on an axis at 90° to the initial axis of deformation. If we consider for simplicity the locus describing intergranular fracture to be fixed in stress space, then the yield surface can be expanded and translated relative to the locus for intergranular fracture in the manner described in Fig. 16 for biaxial tension.

This figure is based on the experimental work of Martin (1982). Clearly, in principle, a strain path can be devised in order to use a sequence of incremental deformation along various axes so as to avoid contact with the locus of intergranular fracture and thus expand the total ductility of the material.

CONCLUSIONS

This work emphasizes two important aspects of the fracture behaviour of materials.

First, it has been shown that the process of damage accumulation leading to ductile fracture can be controlled in several ways: i) by monitoring the strength of the particle-matrix interfacial strength, together with a control of the shape of the particle size distribution, it is possible either to delay or accelerate the nucleation of voids; ii) by superimposing on hydrostatic pressure during the deformation of a material, it is possible to retard damage accumulation, and, therefore, final failure, as this occurs when a critical amount of damage is reached.

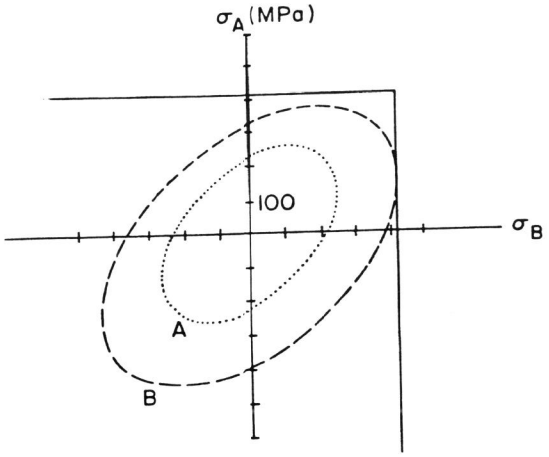

Fig. 16. Yield surface displacement for the peak aged Al-3.6% Cu. Material deformed in tension A and at 90° in compression B.

Secondly, failure maps have been developed to quantify the competition between various fracture modes when variables such as microstructure, superimposed pressure or testing temperature are changed. Despite the simplicity of the models used to plot these maps, they reveal in a pictorial manner the complex interaction between competing fracture mechanisms, and the underlying physical origins, and can also help show how processing variables and strain paths can change the fracture mode of a material.

ACKNOWLEDGEMENT

The authors wish to thank Dr. O. Richmond, Alcoa, U.S.A. and Dr. W. . Spitzig, U.S. Steel, and Mrs. N. Martin for valuable discussions.

They also gratefully acknowledge the research support provided by NSERC Canada and a Dalley Fellowship from McMaster University.

REFERENCES

Ashby, M.F., J.D. Embury, S.H. Cooksley and D. Teirlinck. Scripta Met., to be published.
Thomason, P.F. (1968). J. Inst. Metals, 98, 360.
McClintock, F.A. (1968). J. Appl. Mech., 35, 363.
Brown, L.M. and J.D. Embury (1973). Proc. 3rd Int. Conf. Strength of Metals and Alloys (Cambridge, England), 164.
Brownrigg, A., W.A. Spitzig, O. Richmond, D. Teirlinck and J.D. Embury (1983). Acta Met., 31, 1141.
Palmer, I.G. And G.C. Smith (1966). In Oxide Dispersion Strengthening, Gordon & Breach, New York, 253.
Fisher, J.R. and J. Gurland, (1981). Metals Sci., 15, 185.
Goods, S.H. and L.M. Brown (1979). Acta Met., 27, 1.
Teirlinck, D. (1983). Ph.D. Thesis, McMaster University.
Rice, J.R. and D.M. Tracey (1969). J. Mech. Phys. Solids, 17, 201.

LeRoy, G.H., J.D. Embury, G. Edward and M.F. Ashby (1981). Acta Met., 29, 1509.
Kot, R.A. and J.W. Morris (1979). Editors of Structure and Properties of Dual-Phase Steels, Metallurgical Society of AIME.
Rastogi, P.K. and A.J. Ardell (1971). Acta Met., 19, 321.
Miyoshi, E., M. Fukuda, H. Iwanaga and T. Okazawa (1974). Conf. on Crack Propagation in Pipelines, Inst. of Gas, U.K.
Wilkinson, D.S. and C.H. Caceres. Acta Met., to be published.
Iricibar, R. C.H. LeRoy and J.D. Embury (1980). Metals Sci., 14, 337.
Bridgman, P.W. (1952). In Studies in Large Plastic Flow and Fracture, McGraw-Hill, New York.
Davidson, T.E. and G.S. Ansell (1968). Trans. ASM, 61, 242.
Richmond, O. and W.A. Spitzig (1980). Proc. 15th Int. Cong. of Theoretical and Applied Mechanics, (Toronto, Canada).
McClintock, F.A. (1968). In Ductility, ASM, Metals Park, Ohio, 255.
Murrell, S.A.F. (1983). In Rocks Mechanics, Proc. 5th Symp. Rocks Mech., Ed. C. Fairhurst, Pergamon Press. 563.
Knott, J.F. (1973). In Fundamentals of Fracture Mechanics, John Wiley and Sons, New York.
Fisher, J.C., E.W. Hart and R.H. Pry (1953). Acta Met., 1, 336.
Brown, L.M. and W.M. Stobbs (1971). Phil. Mag., 23, 1185.
Moan, G.D. and J.D. Embury (1979). Acta Met., 27, 903.
Martin, N. (1982). M.Eng. Thesis, McMaster University.